

A comparative study on thermoelectric properties of ZnO bulks and thin films

Dai Cao Truong^{1,2}, Anh Tuan Thanh Pham^{2,3,*}, Oanh Truong Kieu Le^{2,3}, Dung Van Hoang^{1,2,3},
Truong Huu Nguyen^{2,3}, Hanh Kieu Thi Ta^{1,2,4}, Ngoc Kim Pham^{1,2,4}, Hoa Thi Lai^{1,2}, Thang Bach Phan^{1,2,3},
Vinh Cao Tran^{2,3}



Use your smartphone to scan this QR code and download this article

¹Center for Innovative Materials and Architectures (INOMAR), HoChiMinh City, Vietnam

²Vietnam National University, HoChiMinh City, Vietnam

³Laboratory of Advanced Materials, University of Science, HoChiMinh City, Vietnam

⁴Faculty of Materials Science and Technology, University of Science, HoChiMinh City, Vietnam

Correspondence

Anh Tuan Thanh Pham, Vietnam National University, HoChiMinh City, Vietnam

Laboratory of Advanced Materials, University of Science, HoChiMinh City, Vietnam

Email: pttanh@hcmus.edu.vn

History

- Received: 2020-09-07
- Accepted: 2020-11-25
- Published: 2020-12-16

DOI : 10.32508/stdj.v23i4.2458



Copyright

© VNU-HCM Press. This is an open-access article distributed under the terms of the Creative Commons Attribution 4.0 International license.



ABSTRACT

Introduction: Zinc oxide (ZnO) is well-known as a promising thermoelectric material owing to its safety, inexpensiveness, and thermal stability. This research provides an overview of thermoelectric potentials, including structure, electrical conductivity, Seebeck coefficient, and power factor of pure ZnO semiconductor synthesized in bulk and thin-film forms. **Methods:** The ZnO bulk was synthesized by solid-state reaction at high temperature, while the thin film was prepared by d.c. magnetron sputtering technique. The temperature-dependent thermoelectric properties of all the samples were measured by the Seebeck LSR-3 system. The crystallographic and surface morphological information of the samples were obtained by using X-ray diffraction (XRD) and field-emission scanning electron microscopy (FESEM), respectively. **Results:** The XRD results confirm that both the bulk and thin-film have polycrystalline structure and characteristics of hexagonal-wurtzite ZnO. Through the FESEM observation, the bulk is well densified under high-temperature condition, while the thin-film achieve good orientation and close-packed grains. At 573 K, the obtained thermoelectric properties (electrical conductivity, Seebeck coefficient, and power factor) are respectively 352.4 S/cm, -89.5 μ V/K and 282.5 μ W/mK² for the ZnO bulk; and 289 S/cm, -113.8 μ V/K and 374.3 μ W/mK² for the ZnO film. **Conclusion:** The comparative study shows the good thermoelectric potential of ZnO material in both forms of bulk and thin film. Among them, the thin film has better results, especially in the Seebeck coefficient and power factor than one.

Key words: Thermoelectrics, ZnO, bulks, thin films, power factor

INTRODUCTION

At present, energy deficiency, air pollution, and global warming are essential problems in human lives and production activities. One of the important solutions is to explore renewable energy resources alternative for fossil fuels with low efficiency of energy production due to heat loss. Thermoelectrics (TE) emerges as a potential candidate that has attracted a massive number of scientists over the world^{1,2}. TE materials are well-known to convert waste heat directly to electricity according to the Seebeck effect. This technology has a lot of advantages, such as eco-friendliness, noiselessness, durability, and simple structure³⁻⁵.

With the aim to harvest electricity from large waste-heat sources such as metallurgical industrial furnaces, petroleum exploitation, and transportation vehicles⁴, high electrical power is believed to produce. A characteristic quantity for the power production ability of a TE material is a power factor (PF) defined as $PF = \sigma S^2$, where σ and S are electrical conductivity and Seebeck coefficient, respectively. Among TE materials, ZnO possesses preminent properties such as rela-

tively high Seebeck coefficient, inexpensiveness, non-toxicity, and stability at high temperature^{6,7}. However, these properties of the pure ZnO material vary and depend significantly on dopants and structure (bulk and nanostructures). Recently, there has been a lot of studies on nanostructure-based ZnO materials, including nanorods, thin films, and nanoparticles because of their high conductivity and Seebeck coefficient⁸⁻¹¹. Additionally, in forms of nanostructures, typically thin films, their TE characteristics can be controlled by changing thickness, structure, shape, and chemical stoichiometry^{9,12}. In this work, we compare the crystalline structural, morphological, and TE properties, especially the power factor of the ZnO bulk and thin film, which has not been reported previously.

MATERIALS – METHODS

ZnO powder (99.9%, Merck, Germany) was used to synthesize the bulk sample by using the conventional solid-state reaction method. The mixture of the powder and distilled water with a ratio of 1:1 was ground

Cite this article : Truong D C, Pham A T T, Le O T K, Hoang D V, Nguyen T H, Ta H K T, Pham N K, Lai H T, Phan T B, Tran V C. **A comparative study on thermoelectric properties of ZnO bulks and thin films.** *Sci. Tech. Dev. J.*; 23(4):793-799.

in 5 hours by using planetary ball-milling with a speed of 300 rpm (Ceramic Instruments Srl, Italy). After the wet ball-milling process, the powder slurry was dried, cold-pressed at 14 MPa into $30 \times 30 \times 5 \text{ mm}^3$ pellet, and then sintered at 1400°C in 3 hours.

By using the same synthesis route, a 3-inch ZnO ceramic pellet was employed as a sputtering target for thin-film deposition. The 1000-nm-thick ZnO film was deposited on a Corning glass substrate (Eagle XG, Korea) by using d.c. magnetron sputtering technique (Leybold Univex-450, Germany), in pure Ar atmosphere. The substrate temperature, working pressure, and sputtering power were fixed at 300°C , 3.5 mtorr, and 60 W, respectively.

The bulk and film-on-substrate samples were cut into $2 \times 2 \times 15 \text{ mm}^3$ and $5 \times 15 \times 1 \text{ mm}^3$ pieces, respectively, for measuring temperature-dependent electrical conductivity and Seebeck coefficient (Linseis LSR-3, Germany). From these data, the power factor of the samples was calculated. Crystalline structure of the samples was analyzed by using X-ray diffraction method (XRD, Bruker D8-Advance, Japan), with $\text{CuK}\alpha$ X-ray source ($\lambda = 0.154 \text{ \AA}$) and θ - 2θ configuration. The surface morphology of the samples was observed by using field-emission scanning electron microscopy (FESEM, Hitachi S4800, Japan). The carrier concentration of the samples was obtained from Hall measurement (Ecopia HMS3000, Korea) at room temperature. The measurement of bulk density is based on Archimedes' method by using an electronic weighing balance with error margin of 0.1 mg (Sartorius BSA 224S-CW, Germany), combining with a density determination kit (Sartorius YDK03, Germany).

RESULTS

Figure 1 shows that the ZnO bulk has crystal growth along many different planes, which are in accordance with the characteristic structure of the wurtzite-ZnO (JCPDS No. 36-1451). In contrast, only one crystalline orientation along (002) plane perpendicular to the substrate is observed in the XRD pattern of the ZnO film. The results are completely in line with the others^{2,13}. The XRD intensity in the pattern of the film is much higher than that of the bulk, indicating better crystalline orientation in the ZnO film. To estimate crystallinity of the samples quantitatively, however, average crystal size (D) is calculated from the Debye-Scherrer's formula as given by $D = 0.9\lambda/(\beta\cos\theta)$, where $\lambda = 0.154 \text{ nm}$ is the X-ray wavelength, β is the full width at half maximum, and θ is the Bragg diffraction angle. The crystallographic data of the samples are listed in Table 1.

The average crystal sizes along the (100), (002), (101), (102), and (110) planes for the bulk and along the (002) for the film are calculated in Table 1. The results show that the bulk has larger crystal sizes than the film, regardless of different orientations. It suggests that despite worse crystalline preferred orientation, the bulk still has better crystallinity as compared to the film, due to the direct sintering from powder particles at high temperature. This result can be confirmed through the morphology observation of the samples in Figure 2.

Figure 2 shows the surface morphology of the two samples. The ZnO bulk has good densification as a result of sintering at 1400°C ¹. The bulk density is found to be 5.073 g/cm^3 equaling 90.5% of the theoretical density of ZnO (5.606 g/cm^3)¹⁴. The crystalline grains have random shapes, unclear boundaries, and large sizes from several to tens of micrometers. However, there are some interstitial voids between grains, which is known as a drawback of the solid-state reaction method. The formation of the voids can also originate from the size of the precursor ZnO powder particle. By the mechanical wet ball-milling technique, the limited particle size can be obtained about $1 \mu\text{m}$ ¹⁵. The larger powder particle size is, the much interstitial voids create. On the other hand, the ZnO film has polyhedral grains, clear grain boundaries, and average grain size of approximately 200 nm, which is much smaller than that of the bulk sample. Unlike the bulk, the surface morphology of the film is uniform, close-packed without interstitial voids.

Next, residual stress (ϵ) in the samples is considered as given by¹⁰:

$$\epsilon = \left[\frac{2C_{13}^2 - C_{33}(C_{11} + C_{12})}{2C_{13}} \right] \left(\frac{c_s - c_o}{c_o} \right) \quad (1)$$

where C_{ij} are the elastic constants for ZnO ($C_{13}=104.2 \text{ GPa}$, $C_{33} = 213.8 \text{ GPa}$, $C_{12}= 119.7 \text{ GPa}$ and $C_{11}=208.8 \text{ GPa}$), c_s and $c_o = 5.2066 \text{ \AA}$ are the lattice constants "c" of the samples and the standard ZnO, respectively. The "c" constant of the samples is calculated from the Bragg's law defined as $\lambda = 2d \sin \theta = c \sin \theta$, where $d = c/2$ is the interplanar spacing of the hexagonal ZnO{002} planes¹⁶. Besides, the "a" constant of the bulk sample is derived from $d = a$ for the ZnO{100} planes. The calculated results are shown in Table 2.

It is seen that the small difference in "c" constant can give rise to a significant difference in residual stress between the bulk and film samples. The positive stress

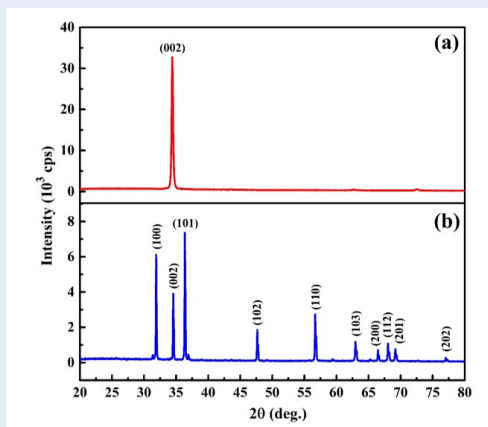


Figure 1: XRD patterns of the ZnO (a) film, and (b) bulk samples. The identification of crystalline planes is confirmed by the standard XRD pattern of ZnO powder (JCPDS No. 36-1451).

Table 1: The crystal sizes along the main preferred orientations of the ZnO bulk and film

Planes	ZnO bulk					ZnO film
	(100)	(002)	(101)	(102)	(110)	(002)
2θ (deg.)	31.88	34.57	36.36	47.65	56.69	34.39
β (deg.)	0.1280	0.1263	0.1530	0.1279	0.1280	0.2515
D (nm)	65.52	65.98	54.03	68.87	71.58	33.05

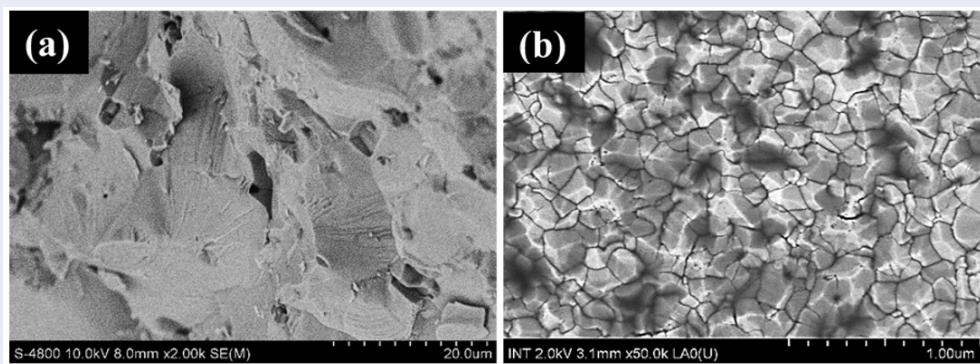


Figure 2: FESEM images of the ZnO (a) bulk, and (b) film samples. The surface morphologies of the two samples are relatively uniform, with different densification and grain size.

Table 2: Lattice constants and residual stress of the ZnO bulk and film

Samples	Lattice constant		Residual stress (GPa)	
	a (Å)	c (Å)		
Bulk	3.240	5.184	4.99	Tensile
Film	-	5.212	-1.36	Compressive

means the existence of tensile stress in bulk, whereas the negative stress shows compressive stress in the film sample. The tensile stress in bulk can be explained in terms of oxygen evaporation from ZnO particle surface during the high-temperature sintering process⁵. The increase in oxygen vacancies results in the shrunk unit cell. On the other hand, the compressive stress in the film is mainly attributed to the lattice mismatch between the film and the substrate.

Figure 3 illustrates the variation of electrical conductivity of the samples as a function of temperature. It is seen that the opposite tendency between the two samples. The conductivity of the film increases slightly 280.5 to 289.0 S/cm with increasing temperature from 300 to 573 K, which behaves as a semiconductor. Furthermore, the obtained value of the film is higher than that of the other reports, as listed in **Table 3**. It can be due to its stability at high temperatures, good orientation, and close-packed structure, which is mentioned above in the FESEM analysis. In contrast, the decreased conductivity from 424.4 to 352.4 S/cm versus the temperature of the bulk characterizes a degenerated semiconductor.

Figure 4 exhibits the variation of Seebeck coefficient of the samples as a function of temperature. All the Seebeck coefficients are negative, which reflects the n-type semiconductor behavior of the two samples. Except at 300 K for the bulk, the increased rate in Seebeck coefficient versus temperature of the two samples is quite similar. When the temperature increased from 300 to 573 K, the $|S|$ value increases from 43.8 to 89.5 $\mu\text{V/K}$, and from 79.9 to 113.8 $\mu\text{V/K}$ for the bulk and film samples, respectively. The value of Seebeck coefficient tends to be inversely proportional to the conductivity, which will be discussed later.

Figure 5 shows the variation of the power factor of the samples as a function of temperature. The power factor of the two samples tends to increase significantly with increasing temperature. At 573 K, the highest power factor can be achieved 282.5 $\mu\text{W/mK}^2$ and 374.3 $\mu\text{W/mK}^2$ for the bulk and film samples, respectively. The high power factor is a combination of high Seebeck coefficient and/or high electrical conductivity. Consequently, the better power factor of the film as compared to that of the bulk is mainly decided by the Seebeck coefficient.

DISCUSSION

As mentioned in **Figure 3**, the electrical conductivity of the bulk is completely higher than that of the film over the investigated temperature range. It is due to the good crystallinity with large grain size and fewer grain boundaries in the bulk sample, which is

indicated in the XRD (**Figure 1**) and FESEM results (**Figure 2**). Another problem is that the ZnO bulk has higher electrical conductivity but a lower Seebeck coefficient as compared to the ZnO film. To understand the trade-off between σ and S values, the Pisarenko's relation is considered as²¹:

$$S = \frac{8\pi^2 k_B^2}{3eh^2} m_d^* T \left(\frac{\pi}{3n} \right)^{2/3} \quad (2)$$

where k_B is the Boltzmann constant, h is the Planck constant, e is the elementary charge, m_d^* is the density-of-state effective mass, T is the temperature, and n is the carrier concentration. In **Figure 3**, it is seen that the temperature-dependent conductivity of the two samples depends strongly on carrier concentration regardless of degenerated or non-degenerated behaviors. Thus, the carrier concentration can be a major factor controlling the conductivity and Seebeck coefficient. The values of carrier concentration at room temperature of the samples are typically checked and listed in **Table 4**.

It is clearly seen that the high carrier concentration can be responsible for the high conductivity of the bulk. Furthermore, based on equation (2), the Seebeck coefficient is inversely proportional to the carrier concentration. Thus, the bulk with a higher n -value also has a lower $|S|$ value, as compared to the film sample. As a result, the trade-off between σ and $|S|$ values of the ZnO bulk and film samples is demonstrated.

Another characteristic of the ZnO film is that both its conductivity and its Seebeck coefficient increase with increasing temperature. It can be explained in terms of the energy filtering effect, which is an interesting effect in low-dimensional or nano-structures^{22,23}. Under thermal impact, the conductivity of the film increases because defect-induced carrier concentration increases. The low-energy carriers can be suppressed by potential barriers at grain boundaries, which exist much in the ZnO film. It leads to large charge accumulation, high potential difference and thus increases the Seebeck coefficient. As a result, the power factor of the ZnO film is significantly enhanced.

CONCLUSION

In this work, the crystalline structure, surface morphology, and thermoelectric properties of the ZnO bulk and thin film are investigated and compared. The ZnO bulk is synthesized through solid-state reaction while the ZnO film is deposited by the sputtering technique. The trade-off between electrical conductivity and Seebeck coefficient of the samples is indicated through the opposite dependence on carrier concentration. In which, the film has lower conductivity but

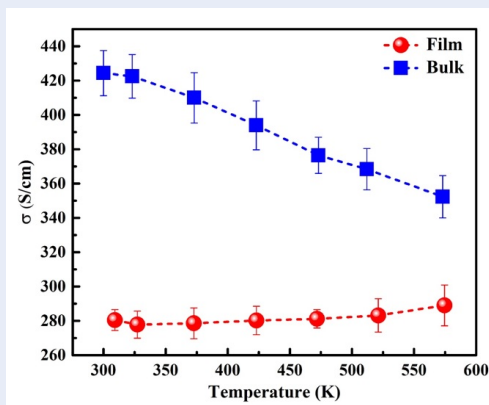


Figure 3: Temperature-dependent electrical conductivity of the ZnO bulk and film. The variation tendency in conductivity of the two samples tends to be opposite. The error margins of the conductivity and temperature are approximately 5%.

Table 3: Comparison of electrical conductivity of some works on ZnO thin films

Methods	Measuring temperature (K)	Electrical conductivity (S/cm)	Ref.
Solgel	300	7.19	17
Solgel	473	4.5	18
Chemical spray pyrolysis	300	0.015	19
Ion beam sputtering	300	100	20
DC magnetron sputtering	383	52.5	10
DC magnetron sputtering	300	6.25	16
DC magnetron sputtering	573	289.0	This work

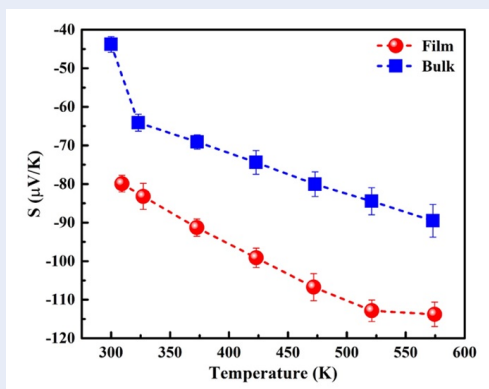


Figure 4: Temperature-dependent Seebeck coefficient of the ZnO bulk and film. The $|S|$ values of the two samples tend to increase with increasing temperature. The error margins of the Seebeck coefficient and temperature are approximately 5%.

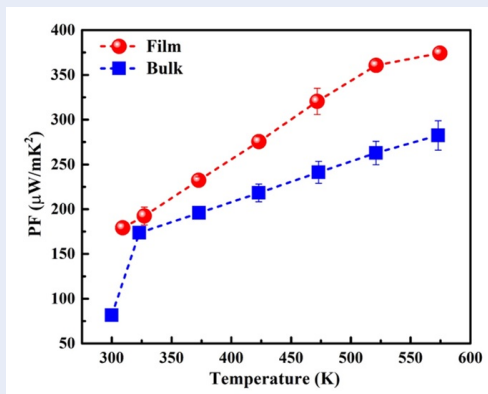


Figure 5: The temperature-dependent power factor of the ZnO bulk and film. The power factors of the two samples tend to increase monotonically with increasing temperature. The error margins of the power factor and temperature are approximately 5%.

Table 4: Room-temperature carrier concentration, electrical conductivity, and Seebeck coefficient of the ZnO bulk and film samples

Samples	n (10 ¹⁹ cm ⁻³)	σ (S/cm)	S (μV/K)
Bulk	6.4 ± 0.3	424.4 ± 13.2	43.8 ± 2.0
Film	4.3 ± 0.2	280.5 ± 6.1	79.9 ± 2.2

higher Seebeck coefficient, as compared to the bulk. Furthermore, combining with the energy filtering effect, the ZnO film achieved the highest power factor (374.3 μW/mK²), which enhanced by 33% as compared to that (282.5 μW/mK²) of the ZnO bulk at 573 K.

LIST OF ABBREVIATIONS

σ: Electrical conductivity
 n: Carrier concentration
 PF: Power factor
 S: Seebeck coefficient
 TE: Thermoelectric
 XRD: X-ray diffraction
 ZnO: Zinc oxide

COMPETING INTERESTS

The authors declare that they have no competing interests.

AUTHOR'S CONTRIBUTIONS

Dai Cao Truong prepared the samples and wrote the draft. Anh Tuan Thanh Pham conceived the idea, revised and completed the manuscript. Oanh Kieu Truong Le, Dung Van Hoang, Truong Huu Nguyen, Hanh Kieu Thi Ta, Ngoc Kim Pham, Hoa Thi Lai performed the measurements. Vinh Cao Tran and Thang Bach Phan led the research group. All the authors have approved contents of the final version.

ACKNOWLEDGMENTS

This work was supported by the Vietnam Ministry of Science and Technology under grant number ĐTĐL.CN-23/18.

REFERENCES

- Pham ATT, Luu TA, Pham NK, Ta HKT, Nguyen TH, Hoang DV, et al. Multi-scale defects in ZnO thermoelectric ceramic materials co-doped with In and Ga. *Ceram Int.* 2020;46(8):10748–10758. Available from: <https://doi.org/10.1016/j.ceramint.2020.01.084>.
- Radingoana PM, Guillemet-Fritsch S, Noudem J, Olubambi PA, Chevallier G, Estournès C. Thermoelectric properties of ZnO ceramics densified through spark plasma sintering. *Ceram Int.* 2020;46(4):5229–5238. Available from: <https://doi.org/10.1016/j.ceramint.2019.10.271>.
- Tan G, Zhao LD, Kanatzidis MG. Rationally designing high-performance bulk thermoelectric materials. *Chem Rev.* 2016;116(19):12123–12149. PMID: 27580481. Available from: <https://doi.org/10.1021/acs.chemrev.6b00255>.
- Aswal DK, Basu R, Singh A. Key issues in development of thermoelectric power generators: High figure-of-merit materials and their highly conducting interfaces with metallic interconnects. *Energy Convers Manag.* 2016;114:50–67. Available from: <https://doi.org/10.1016/j.enconman.2016.01.065>.
- Vogel-Schäuble N, Dujardin R, Weidenkaff A, Aguirre MH. Influence of thermal aging phenomena on thermoelectric properties of Al-substituted ZnO. *J Electron Mater.* 2012;41(6):1606–1614. Available from: <https://doi.org/10.1007/s11664-011-1851-2>.
- Wang C, Wang Y, Zhang G, Peng C. Electronic structure and thermoelectric properties of ZnO single-walled nanotubes

- and nanowires. *J Phys Chem C*. 2013;117(41):21037–21042. Available from: <https://doi.org/10.1021/jp403827n>.
7. Zhao Y, Wang J, Huxtable S, Khodaparast GA, Priya S. Role of sintering atmosphere and synthesis parameters on electrical conductivity of ZnO. *Energy Harvest Syst*. 2015;2(1-2). Available from: <https://doi.org/10.1515/ehs-2015-0002>.
 8. Loureiro J, Neves N, Barros R, Mateus T, Santos R, Filonovich S, et al. Transparent aluminium zinc oxide thin films with enhanced thermoelectric properties. *J Mater Chem A*. 2014;2(18):6649–6655. Available from: <https://doi.org/10.1039/C3TA15052F>.
 9. Vineis CJ, Shakouri A, Majumdar A, Kanatzidis MG. Nanostructured thermoelectrics: big efficiency gains from small features. *Adv Mater*. 2010;22(36):3970–3980. PMID: 20661949. Available from: <https://doi.org/10.1002/adma.201000839>.
 10. Nguyen NHT, Nguyen TH, Liu Y, Aminzare M, Pham ATT, Cho S, et al. Thermoelectric properties of Indium and Gallium dually doped ZnO thin films. *ACS Appl Mater Interfaces*. 2016;8(49):33916–33923. PMID: 27960402. Available from: <https://doi.org/10.1021/acsmi.6b10591>.
 11. Fan P, Li YZ, Zheng ZH, Lin Q, Luo J, Liang G, et al. Thermoelectric properties optimization of Al-doped ZnO thin films prepared by reactive sputtering Zn-Al alloy target. *Appl Surf Sci*. 2013;284:145–149. Available from: <https://doi.org/10.1016/j.apsusc.2013.07.070>.
 12. Kim S, Kim D, Byeon J, Lim J, Song J, Park S, et al. Transparent amorphous oxide semiconductor as excellent thermoelectric materials. *Coatings*. 2018;8(12). Available from: <https://doi.org/10.3390/coatings8120462>.
 13. Zhou Z-F, Ren G-K, Tan X, Liu R, Liu C, Lin Y-H, et al. Enhancing the thermoelectric performance of ZnO epitaxial films by Ga doping and thermal tuning. *J Mater Chem A*. 2018;6(47):24128–24135. Available from: <https://doi.org/10.1039/C8TA06824K>.
 14. Mazaheri M, Zahedi AM, Sadrnezhad SK. Two-step sintering of nanocrystalline ZnO compacts: Effect of temperature on densification and grain growth. *J Am Ceram Soc*. 2008;91(1):56–63. Available from: <https://doi.org/10.1111/j.1551-2916.2007.02029.x>.
 15. Lalena JN, Cleary DA, Carpenter E, Dean NF. *Inorganic materials synthesis and fabrication*. New York: John Wiley & Son. 2007;p. 312. Available from: <https://doi.org/10.1002/9780470191576>.
 16. Pham ATT, Nguyen PAT, Phan YKT, Nguyen TH, Hoang DV, Le OKT, et al. Effects of B2O3 doping on the crystalline structure and performance of DC-magnetron-sputtered, transparent ZnO thin films. *Appl Opt*. 2020;59(19):5845. PMID: 32609712. Available from: <https://doi.org/10.1364/AO.395051>.
 17. Benramache S, Benhaoua B, Belahssen O. The crystalline structure, conductivity and optical properties of Co-doped ZnO thin films. *Optik*. 2014;125(19):5864–5868. Available from: <https://doi.org/10.1016/j.ijleo.2014.07.055>.
 18. Hong M-H, Park C-S, Seo W-S, Lim YS, Lee J-K, Park H-H. Thermoelectric properties of Al-doped mesoporous ZnO thin films. *J Nanomater*. 2013;2013:1–6. Available from: <https://doi.org/10.1155/2013/131537>.
 19. Hadri A, Taibi M, Loghmarti M, Nassiri C, Slimani TT, Mzard A. Development of transparent conductive indium and fluorine co-doped ZnO thin films: Effect of F concentration and post-annealing temperature. *Thin Solid Films*. 2016;601:7–12. Available from: <https://doi.org/10.1016/j.tsf.2015.11.036>.
 20. Kennedy J, Murmu PP, Leveneur J, Leveneur J, Williams VM, Moody RL, et al. Enhanced power factor and increased conductivity of aluminum doped zinc oxide thin films for thermoelectric applications. *J Nanosci Nanotechnol*. 2018;18(2):1384–1387. PMID: 29448596. Available from: <https://doi.org/10.1166/jnn.2018.14105>.
 21. Tanusilp S, Nishide A, Ohishi Y, Muta H, Hayakawa J, Kurosaki K. High thermoelectric power factor of ytterbium silicon-germanium. *Appl Phys Lett*. 2018;113(19):193901. Available from: <https://doi.org/10.1063/1.5047091>.
 22. Thesberg M, Kosina H, Neophytou N. On the effectiveness of the thermoelectric energy filtering mechanism in low-dimensional superlattices and nano-composites. *J Appl Phys*. 2016;120(23):234302. Available from: <https://doi.org/10.1063/1.4972192>.
 23. Narducci D, Selezneva E, Cerofolini G, Frabboni S, Ottaviani G. Impact of energy filtering and carrier localization on the thermoelectric properties of granular semiconductors. *J Solid State Chem*. 2012;193:19–25. Available from: <https://doi.org/10.1016/j.jssc.2012.03.032>.